The International Journal of Advanced Manufacturing Technology (2018) 98:2401–2413
https://doi.org/10.1007/s00170-018-2389-8

ORIGINAL ARTICLE

A thermal model for hard precision turning

M. A. Shalaby[1,2] · M. A. El Hakim[3] · S. C. Veldhuis[1]

Received: 13 February 2018 / Accepted: 28 June 2018 / Published online: 9 July 2018

Abstract

This work presents a developed thermal model of hard precision turning, in which the depth of the cut is made to be considerably smaller than the tool nose radius for final finishing. The required input data for this model was extracted from a previously published mechanistic model of precision turning. This mechanistic model is based on Merchant's analysis of 3D cutting, which was modified to adopt the precision turning operation. Calculations were obtained of the shear plane temperature rise at the primary deformation zone and the temperature rise of the chip due to the work done in overcoming friction at the secondary deformation zone (frictional temperature rise). The thermophysical properties of the workpiece and cutting tool materials as well as their variation under different shear plane and frictional temperatures were considered. After performing the required calibrations, the cutting temperatures were measured with the tool-workpiece thermocouple technique during machining of hardened HSS and D2 tool steel by PCBN and mixed alumina ceramic tools. The occurrence of secondary hardening during HSS machining was found to be dependent on the thermal conductivity of the tool material. The estimated cutting temperatures were found to be reasonably close to the measured ones.

Keywords Thermal model · Precision hard turning · Cutting temperature

Nomenclatures

a	*Depth of Cut*
b_1	Undeformed chip width
B_t	Geometrical factor
F_a	Axial force component
F_c	Main cutting force component
F_f	Friction force
F_r	Radial force component
F_s	The component of force along shear plane
h_1	Undeformed chip thickness
h_{av}	Average undeformed chip thickness
L_c	Contact length
MFTW	Machine-fixture-tool-workpiece
P_c	Cutting power
P_f	Power consumed in overcoming friction on tool face
P_s	Power consumed in shear
P_{tf}	Power required to overcome friction between worn tool flank and workpiece surface (at the tertiary deformation zone
Q_{ch}	Amount of heat conducted to the chip
q_f	Frictional heat flux
Q_w	Amount of heat conducted to the workpiece
r	Tool nose radius
R_2	Thermal number
R_z	Average peak to valley surface roughness
s	Feed
v	Cutting speed
v_f	Chip frictional velocity
v_s	Shear velocity
α	Clearance angle
γ	True rake angle
Γ_f	Proportion of frictional energy flowing into the chip
γ_n	Normal rake angle

✉ M. A. Shalaby
shalabym@mcmaster.ca

M. A. El Hakim
mohamed_elhakim@eng.asu.edu.eg

S. C. Veldhuis
veldhu@mcmaster.ca

[1] Department of Mechanical Engineering, Faculty of Engineering, McMaster University, 1280 Main St. West, Hamilton, ON L8S 4L7, Canada

[2] Department of Mechanical Design and Production, Technical Research Center, Cairo, Egypt

[3] Department of Mechanical Design and Production, Faculty of Engineering, Ain Shams University, Cairo, Egypt

Γ_s	Proportion of the deformation heat energy entering the chip through the shear plane
γ_x	Side rake angle
γ_y	Back rake angle
δ_s	Angle that the shear force makes with normal to the cutting edge in this plane
ε	Shear strain on shear plane
θ_c	Cutting temperature
θ_f	Frictional temperature rise
θ_o	Ambient temperature
θ_s	Shear plane temperature rise
ρ_w	Workpiece density
φ_c	Contact angle

1 Introduction

In metal cutting, the energy expended in the primary deformation zone shearing along the shear plane, and in the plastic deformation and friction at the tool-chip interface in the secondary deformation zone, is mostly converted into heat [1]. When a cutting tool edge wears out during machining, the rubbing effect of the workpiece surface against the tool flank in the tertiary deformation zone is another source of heat [2]. Commonly defined as the average temperature measured at the tool-chip interface, cutting temperature resulting from the heat generated during machining has a remarkable effect on the process performance. The greater the cutting speed, feed, and depth of cut, the greater also is the power consumed by the shearing action and plastic deformation, as well as the cutting temperature [3]. Machining a workpiece with greater ultimate strength such as in hardened steels results in greater flow stress of the workpiece material during cutting; therefore, generating an extra amount of heat also raises the cutting temperature [4]. The thermophysical properties of the tool and workpiece such as the thermal conductivity and the volumetric heat capacity affect the cutting temperature, which will be further discussed in the present work.

The workpiece machinability can be assessed by the cutting temperature [5]. An increase of the cutting temperature strongly corresponds with the cutting tool wear and the microstructural changes on the workpiece surface [6, 7]. Raising the cutting temperature decreases the cutting force components through thermal softening of the material at the shear plane [8]. The accuracy of the machine tools and workpieces can be limited by thermally induced deviations. These deviations become important when considering the trends of hard precision cutting [5]. However, because of the small feed and depth of cut used in hard precision turning, the generated heat is concentrated on a small area of the tool-chip interface, which results in a greater rate of tool wear [9]. Tribochemical reactions at the tool-chip interface usually take place in this machining operation, especially under dry conditions, and thus require a study of the cutting temperature results [10, 11]. However, theoretical analysis and experimental measurement of the cutting temperature in dry hard precision turning are needed to explain the aforementioned phenomena encountered during cutting. To that end, the required measurement of the cutting temperature depends on the case under study, such as the available location of the sensor, dynamics of cutting, accuracy needed, and cost of instrumentation. Several methods were used to measure the cutting temperature:

- Embedded thermocouple [12, 13]
- Dynamic thermocouple or tool-workpiece thermocouple [14–16]
- Infrared photography, optical infrared radiation pyrometers [17, 18]
- Thermal paints, materials with a known melting point, either in a powder or thin film form [18]
- High-speed steel tools undergoing microstructural changes alongside cutting temperature [19]

Nevertheless, obtaining access to the tool-chip interface is technically difficult in most of the used techniques, especially for precision hard turning due to the small chip area. Therefore, the tool-workpiece thermocouple can be a reliable method in this case, with the measured values representing the mean temperatures over the tool-chip interface [20]. In this method, the contact region at the tool-chip interface forms a hot junction during cutting, whereas the entire part of the tool-workpiece is used to form the cold junction. An electromotive force (emf) is generated between the tool and the workpiece due to the gradient between the cutting and environmental temperatures. The captured emf chiefly depends on the continuity of the electrical circuit, which makes this technique more suitable in the case of continuous chip formation [21]. Care must be taken to avoid parasitic (secondary) emf, which may arise with tipped tools such as PCBN usually used in hard turning, as well as to prevent short circuiting, which can occur if the chip makes a secondary contact with the tool substrate and/or tool holder [20]. Calibration establishing the necessary relationship between the captured emf and the real cutting temperature is one of the major problems of applying the tool-workpiece thermocouple while measuring the cutting temperature. The most widely used calibration method involves comparing the emf generated by a standard thermocouple immersed in molten lead contained in a thermo-insulated vessel to the emf produced when the tool and the workpiece form another thermocouple in the same container [21]. The workpiece is usually represented by a long chip. This calibration technique is difficult to apply if the workpiece does not produce a long continuous chip such as in the hardened alloy steel and if a tipped tool such as PCBN is used, both of which are the case in this study. Another method is to calibrate the tool-workpiece thermocouple when the tool is in tight contact

with the workpiece surface and the region of contact is heated using an oxygen-acetylene torch. A standard thermocouple is spot welded in the hot area as close as possible to the tool-workpiece contact region [22]. The latter method may not be accurate due to a high probability of generating a secondary emf, which affects the obtained readings. The present study presents a newly developed calibration technique that seeks to avoid the disadvantages of the two aforementioned methods, which will be detailed in the experimental work.

Due to the difficulties associated with the measurements, several modeling methods were applied to predict the cutting temperature. Finite element approaches were applied in thermal modeling of metal cutting [23–25]. These approaches include large formulation that requires relevant friction laws and thermoviscoplastic material behavior at high strain rates and temperatures [2]. Filice et al. [26] and Umbrello et al. [27] mentioned that to achieve an accurate model, a large number of elements are necessary along with refinement and remeshing processes. The calculation time will be only for a limited cutting length; thus, the steady-state cutting cannot be easily simulated.

Analytical models can provide an easier approach to understanding this process and for making improvements. These models are extensively reviewed by Komanduri and Hou [28, 29], usually based on simplifying assumptions that generally focus on a 2D and steady-state orthogonal cutting operation with a simplified tool geometry. Moufki et al. proposed an analytical thermomechanical model including a temperature-dependent friction law at the tool-chip interface [30]. Bahi et al. [31] introduced a more complex friction law that accounted for both sticking and sliding contacts and proposed an analytical-numerical approach. Zhou et al. [32] proposed a model of temperature distribution in the primary shear zone. Li et al. [33] developed a model for dry orthogonal cutting to predict the cutting temperature distribution in the cutting zone. Stephenson [21] found that the most accurate model was that of Loewen and Shaw, because it accounted for the changes in thermal properties of the tool and workpiece with respect to temperature.

In Loewen and Shaw's approach, both primary and secondary shear zones are considered to be planes. The chip and the workpiece are viewed as two bodies in relative motion at the shear plane, and the tool-chip and tool-workpiece contact zones are seen as thermally insulated. Part of the heat delivered to the chip will only stay on the chip and there is no heat flux flowing out of its boundaries [34]. This approach will be used for thermal modeling in the present study after making the necessary modifications.

Hard precision turning is set to partially replace grinding due to its comparable surface roughness and reduction in the total machining cost [9]. Cutting fluids are usually used for machining hard-to-cut alloys [35], and their use can generate significant environmental and health problems [36, 37]. However, hard dry machining becomes a desirable technique in different applications [38].

In the present work, Loewen and Shaw's model will be used to estimate the cutting temperature in dry hard precision turning. Calculations will be performed of the shear plane temperature rise at the primary deformation zone and the temperature rise of the chip due to the work done in overcoming friction at the secondary deformation zone (frictional temperature rise). The required input data for this model will be extracted from a previously published mechanistic model of precision turning [39], based on Merchant's analysis in 3D cutting. Cutting temperature will be measured using the tool-workpiece thermocouple technique.

No previous analytical models have used Loewen and Shaw's approach to estimate the cutting temperature in hard precision turning. This is due to the difficulties associated with the calculations of the undeformed chip thickness and width, which have been addressed in the proposed mechanistic model. In accordance with the mechanistic model, the thermal model in this work can be applied in 3D oblique cutting of precision turning.

To successfully perform the hard cutting operations, superhard tool materials such as PCBN and ceramics are used. These tool materials have different thermal conductivities, which in turn affect the cutting temperature. However, the impact of changing the tool material thermal conductivity on the cutting temperature induced in hard precision turning will be illustrated in this study for the first time.

Secondary hardening, a phenomenon encountered during hard machining of certain high alloy steels, results in an increase of the cutting force components, cutting temperature, and tool wear [40]. A novelty of the present work lies in analyzing the effect of different tool materials with different thermal conductivities on the instances of secondary hardening.

Hardened alloy steels have different thermal conductivity and volumetric heat capacity, depending on their chemical composition. The effects of these two variables on the cutting temperature are to be theoretically and experimentally investigated in the present study.

However, AISI T15 high-speed steel (HSS) and high-chromium, high-carbon tool steel (D2 tool steel) were chosen as the workpiece materials in this study due to their relatively different thermal conductivities and volumetric heat capacities. Moreover, HSS is a representative secondary hardenable high alloy steel. The workpieces' chemical composition are illustrated in Tables 1 and 2. Due to their refractory nature and different thermal conductivities, a low-content PCBN and a mixed alumina ceramic tool were used as tool materials in this investigation. The complete descriptions of the two cutting tools are provided in Tables 3 and 4.

Table 1 Chemical composition of T15 HSS

%C	%Si	%Mn	%Cr	%Mo	%V	%W	%Co	%Fe
1.1	0.2	0.25	4.75	1	5	12.5	5	Balance

Table 2 Chemical composition of AISI D2 tool steel

%C	%Si	%Mn	%Cr	%Mo	%V	%Fe
1.55	0.3	0.4	11.8	0.8	0.8	Balance

2 Modeling of hard precision turning

2.1 Mechanistic model

In precision turning, the tool nose radius is remarkably larger than the depth of cut ($a/r \ll 1$), and low values of feed are used to improve the surface finish and accuracy of the workpiece. However, the classical calculation of the undeformed chip thickness needs to be modified to adopt the precision turning configurations. This has been carried out in the present mechanistic model [39]. The assumptions of this model are as follows: the cutting tool is sharp and unworn during the cutting, the formed chip is continuous with steady frictional action on the tool rake face, a builtup edge is not formed, the chip moves as a rigid body relative to the tool, and the deformation of the chip in the shear plane is uniform. The model's input data are cutting conditions (cutting speed, feed, depth of cut), necessary geometrical features of the cutting tool including the tool nose radius, and the experimentally measured cutting force components (radial, tangential, axial). These data will be utilized to deduce the shear force generated in the primary deformation zone (F_s) and shear velocity in the same zone (v_s) in order to calculate the power consumed during the shearing action. Moreover, the frictional force generated at the secondary deformation zone (F_f) and the chip frictional velocity (v_f) are required to calculate the power consumed during the frictional action. Shear strain (ε) will be also considered in this mathematical work. To extend the mechanistic model to a 3D cutting setting, the measured force components were transferred in the plane of the tool face: along the cutting edge tangent to the tool arc, normal to the tool face, and normal to the cutting edge [34]. A flowchart for the mechanistic model is presented in Fig. 1. The quantities deduced from the mechanistic model will be the input data needed for the developed 3D thermal model.

Table 3 Used PCBN cutting tool

Manufacturer	Sumitomo Electric Carbide, Inc.
Manufacturer's grade name	BNX20
% CBN	55–60
Type of binder	TiN
Hardness at room temperature	3100–3300 Hv
Thermal conductivity at room temperature	50 W/m °C

Table 4 Used mixed alumina ceramic cutting tool

Manufacturer	NTK company
Manufacturer's grade name	HC2
Components	Al_2O_3 (70%) + TiC (30%)
Hardness at room temperature	2000 Hv
Thermal conductivity at room temperature	23 W/m °C

2.2 Thermal model

The power consumed in cutting (P_c) can be expressed as:

$$P_c = P_s + P_f + P_{tf} \quad (1)$$

$$P_c = F_c v \quad (2)$$

$$P_s = F_s v_s \quad (3)$$

P_s is the power required to overcome the shearing resistance at the shear zone (primary deformation zone).

$$P_f = F_f v_f \quad (4)$$

P_f is the power required to overcome the frictional resistance at the chip-tool interface (secondary deformation zone) and P_{tf} is the power required to overcome friction between the worn tool flank and workpiece surface (tertiary deformation zone).

However, unless the tool is severely worn out, which is unacceptable in the precision machining operations, the heat generated due to friction between the worn flank and the workpiece surface is negligible. The power equation can be thus reduced to:

$$P_c = P_s + P_f \quad (5)$$

The cutting power (P_c), which is the rate of mechanical work to overcome the shear and friction, is transformed into an equivalent amount of heat (Q_c), (1 Nm/s = 1 J/s), divided between the chip, the tool, and the workpiece, such that:

$$Q_c = Q_{ch} + Q_w + Q_t \quad (6)$$

Q_{ch} Amount of heat conducted to the chip
Q_w Amount of heat conducted to the workpiece
Q_t Amount of heat conducted to the tool

2.2.1 Temperature in the primary deformation zone

Temperature in the primary shear zone has a great impact on the in-depth study of the cutting process [40]. The produced chip is the first heated by the deformation work overcoming the shear resistance in the primary deformation zone. The shear plane temperature rise (θ_s) is computed as follows [34]:

$$\theta_s = \frac{\Gamma_s P_s}{\rho_w c_w v b_1 h_1} \quad (7)$$

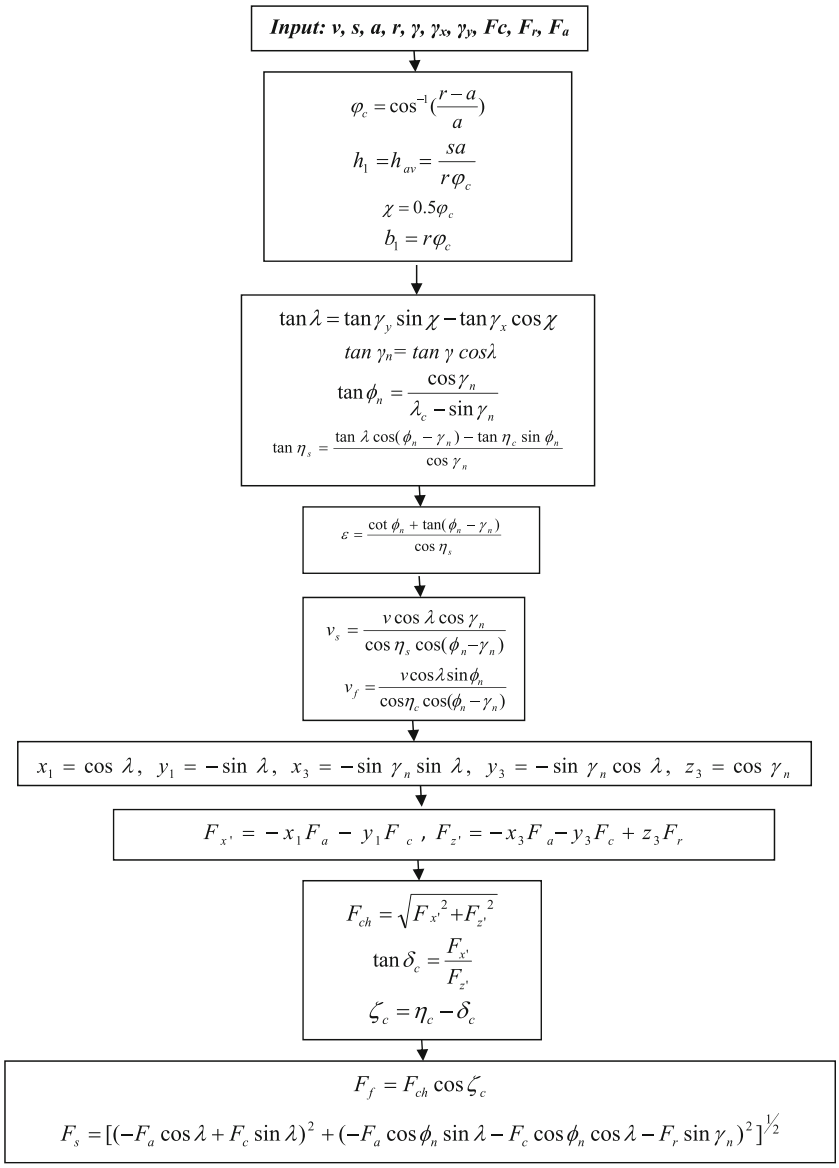

Fig. 1 Flowchart of the mechanistic model used to calculate the necessary quantities for the thermal model

Where (Γ_s) is the proportion of the deformation heat energy entering the chip through the shear plane, given by:

$$\Gamma_s = \frac{1}{1 + 1.328\sqrt{\frac{k_w\varepsilon}{\rho_w c v h_1}}} \tag{8}$$

(ε) is the shear strain in the chip. ρ_w, c_w, and k_w are the density, specific heat, and thermal conductivity of the workpiece material, respectively.

2.2.2 Temperature in the secondary deformation zone

Knowledge of the average temperature rise of the chip due to the work done in overcoming friction at the secondary deformation zone (θ_f) helps in understanding the phenomena encountered at the tool-chip interface. It is given by [34]:

$$\theta_f = \frac{0.377\Gamma_f P}{k b_1\sqrt{R_2}} \tag{9}$$

(Γ_f) is the proportion of frictional energy flowing into the chip, given by:

$$\Gamma_f = \frac{q_f L_c\frac{B_t}{k_t} - \theta_s + \theta_o}{q_f L_c\frac{B_t}{k_t} + 0.377\frac{q_f L_c}{k_w\sqrt{R_2}}} \tag{10}$$

Where (q_f) is the frictional heat flux:

$$q_f = \frac{P_f}{L_c b_2} \tag{11}$$

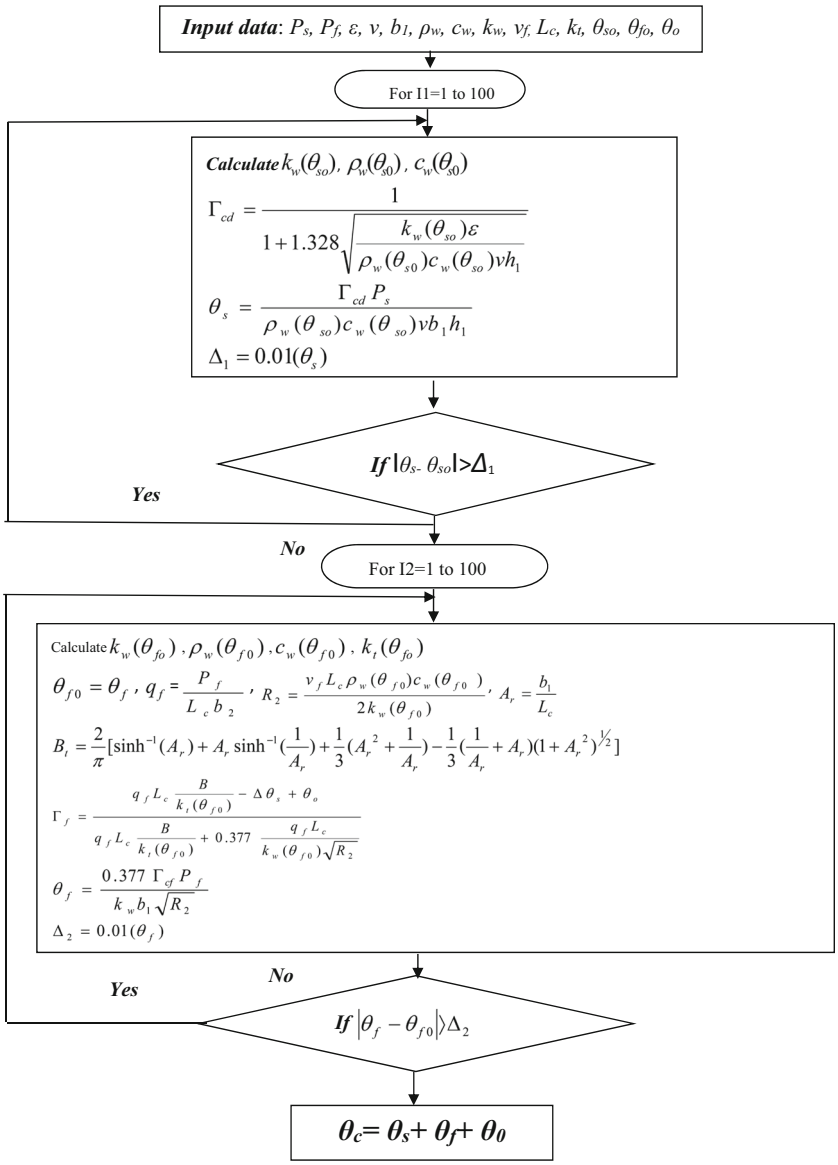

Fig. 2 Flowchart of the cutting temperature calculation

(k_t) is the thermal conductivity of the tool material.

(R_2) is the thermal number for the motion of the chip relative to the tool, given by:

$$R_2 = \frac{v_f L_c \rho_w c_w}{2k_w} \tag{12}$$

(L_c) is the chip contact length on the tool rake face $\approx 2h_{av}$ [41].

$$B_t = \frac{2}{\pi}\left[\sinh^{-1}(A_r) + A_r \sinh^{-1}\left(\frac{1}{A_r}\right) + \frac{1}{3}\left(A_r^2 + \frac{1}{A_r}\right) - \frac{1}{3}\left(\frac{1}{A_r} + A_r\right)\left(1 + A_r^2\right)^{1/2}\right] \tag{13}$$

B_t is a geometrical factor defining the nature of the cutting process, which needs to be identified in precision turning. (A_r) is the aspect ratio of the contact area $= \frac{b_1}{L_c}$ for a tool with a nose radius.

The workpiece material properties (k_w, ρ_w, c_w) and tool thermal conductivity (k_t) are assumed to vary with temperature.

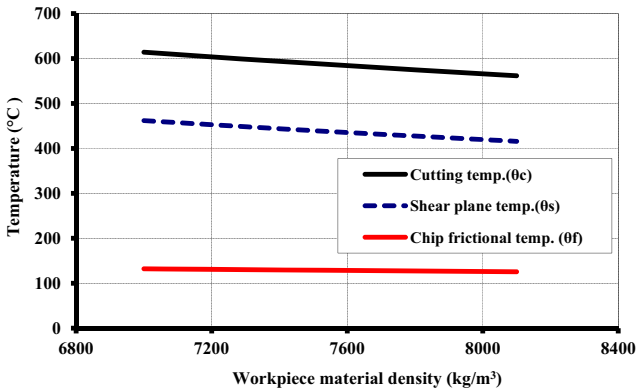

Fig. 3 Effect of the workpiece material density (ρ_w) on the different temperatures

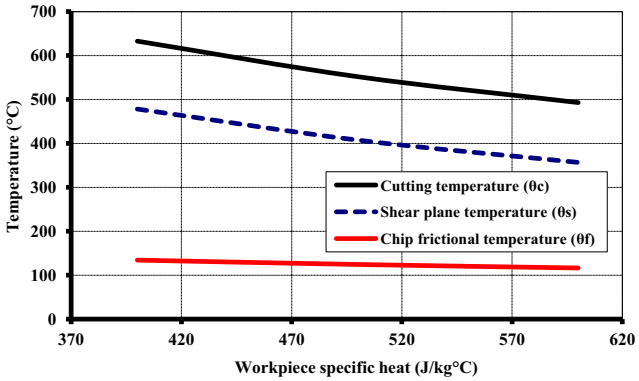

Fig. 4 Effect of the workpiece material specific heat (c_w) on the different temperatures

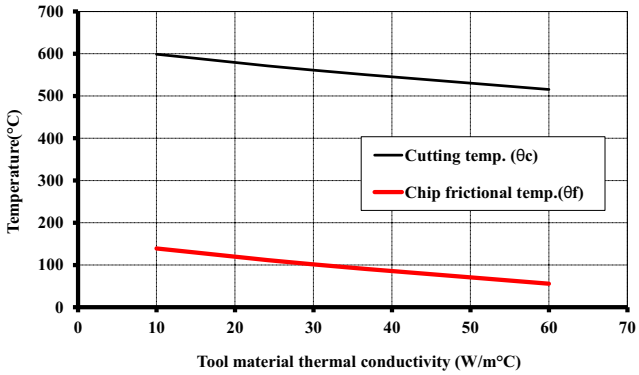

Fig. 6 Effect of the tool material thermal conductivity (k_t) on the chip frictional and cutting temperatures

Iterative calculations are carried out from an initially estimated temperature.

For many metals, the thermal conductivity (k) varies approximately linearly with temperature, whereas the volumetric heat capacity ($\rho\, c$) varies quadratically [22]:

$$k(\theta) = k_o + k_1\theta \tag{14}$$

$$\rho c(\theta) = \rho c_o + \rho c_1\theta + \rho c_2\theta^2 \tag{15}$$

The cutting temperature (θ_c) is therefore obtained as follows:

$$\theta_c = \theta_s + \theta + \theta_o \tag{16}$$

To predict the effects of different workpiece and tool thermophysical properties at the shear plane temperature (θ_s), the frictional temperature (θ_f), and the cutting temperatures (θ_c), the proposed model is applied according to the logical flowchart presented in Fig. 2. The following relationships were deduced from the thermal model:

- Higher workpiece density and specific heat reduce the shear plane temperature but do not remarkably affect the rake face temperature (Figs. 3 and 4). This is a result of the greater amount of heat energy needed to raise the temperature at the shear plane due to the higher volumetric heat capacity ($\rho_w\, c_w$).
- The higher the workpiece thermal conductivity, the higher the rate of heat energy dissipation in the primary and secondary deformation zones. However, machining a workpiece with a higher thermal conductivity (k_w) decreases both the shear plane temperature (θ_s) and the frictional temperature (θ_f) (Fig. 5).
- Using a tool material with a higher thermal conductivity (k_t) decreases the frictional temperature (θ_f) and does not remarkably affect the shear plane temperature (θ_s) (Fig. 6). This is due to the direct contact between the chip and the tool at the frictional region in the secondary deformation zone, which accelerates the heat energy dissipation in this region if using a tool with a higher thermal conductivity.

2.2.3 Effect of temperature rise on the thermophysical properties of the workpiece and tool materials

Figure 7 shows the effect of temperature rise on the thermal conductivity (k_w) for the HSS and D2 tool steel. D2 tool steel has a slightly higher thermal conductivity with increasing temperature starting from 21 to 38 W/m °C, which can be

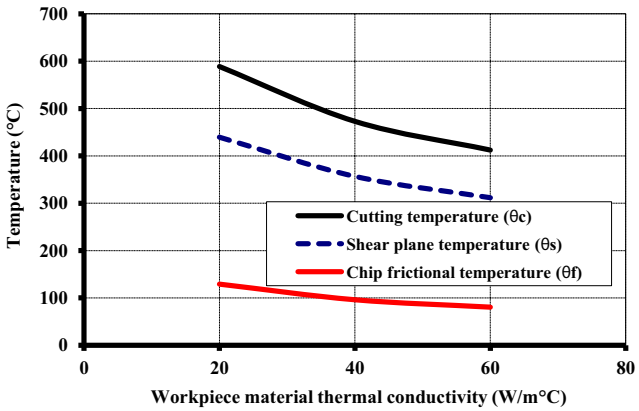

Fig. 5 Effect of the workpiece thermal conductivity (k_w) on the different temperatures

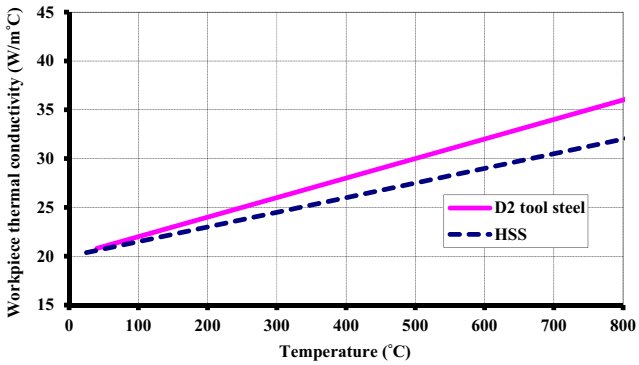

Fig. 7 Effect of the temperature rise on the workpiece thermal conductivity (k_w) for the HSS and D2 tool steel

attributed to its greater chromium content. The HSS material thermal conductivity range is from 20 to 32 W/m °C. The presented values k_w are in the estimated range of shear plane temperature rise.

Figure 8 illustrates the effect of the temperature rise on the different tool materials' thermal conductivity (k_t). PCBN has a higher thermal conductivity, which increases along with temperature, 50 to 55 W/m °C, whereas the mixed alumina ceramic tool has a lower thermal conductivity, which decreases upon an increase of the temperature, 23 to13 W/m °C. These values of k_t are in the expected range of frictional temperature rise.

The effect of temperature rise on the volumetric heat capacity ($\rho_w c_w$) for the HSS and D2 tool steels, in the range of shear plane temperature rise, is presented in Fig. 9. The HSS has a higher volumetric heat capacity at high temperatures than the D2 tool steel due to the exponential relationship of the specific heat (c_w) with respect to temperature [42], whereas this is a quadratic relationship for the D2 tool steel [22].

2.2.4 Estimated temperatures using the developed thermal model

The thermal model aims to estimate the shear plane temperature rise (θ_s) and frictional temperature rise (θ_f) and finally to calculate the resultant cutting temperature (θ_c).

Shear plane temperature rise The estimated shear plane temperatures indicate that the hardened HSS secondary hardening temperature range is 350–600 °C, at which the cutting speed range is 30–50 m/min (Fig. 10a). This range occurs with the mixed alumina ceramic tool at a speed of 30–40 or 40–50 m/min with the PCBN tool. However, secondary hardening occurrence depends on the thermal conductivity of the used tool material. Thus, at the same cutting conditions, secondary hardening is observed at a lower speed range with a tool material that has lower thermal conductivity. This will be explained during the actual measurements of cutting temperatures.

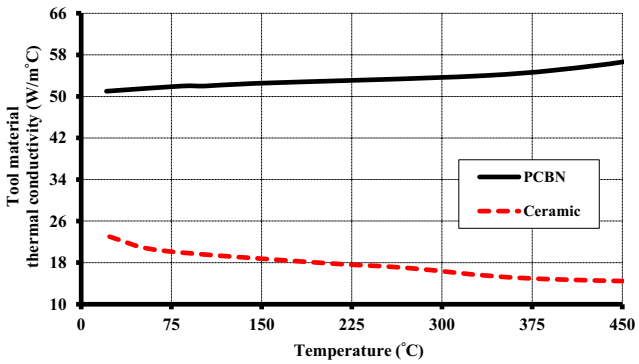

Fig. 8 Effect of the temperature rise on the thermal conductivity (k_t) for the used tool materials

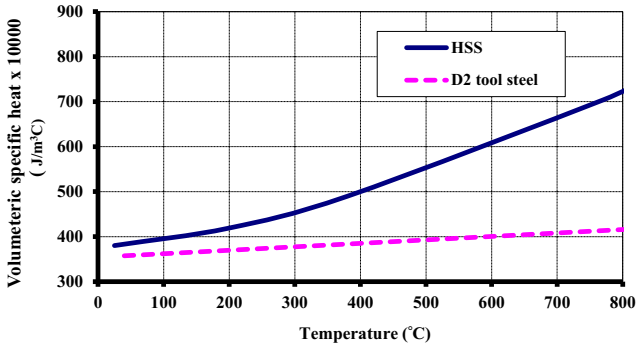

Fig. 9 Effect of the temperature rise on the volumetric heat capacity ($\rho_w c_w$) for the HSS and D2 tool steel

Figure 10b presents the effect of increasing the cutting speed on the shear plane temperature rise for the hardened D2 steel. Due to the lower density (ρ_w) and lower specific heat (c_w), the shear plane temperatures obtained by the D2 steel are higher than those obtained by the hardened HSS presented in Fig. 10a, and this is confirmed in Figs. 3 and 4.

It is notable that in Fig. 10a, b, the mixed alumina ceramic tool demonstrates slightly higher shear plane temperatures during machining of the two workpiece materials at the lower range of cutting speeds, whereas the PCBN

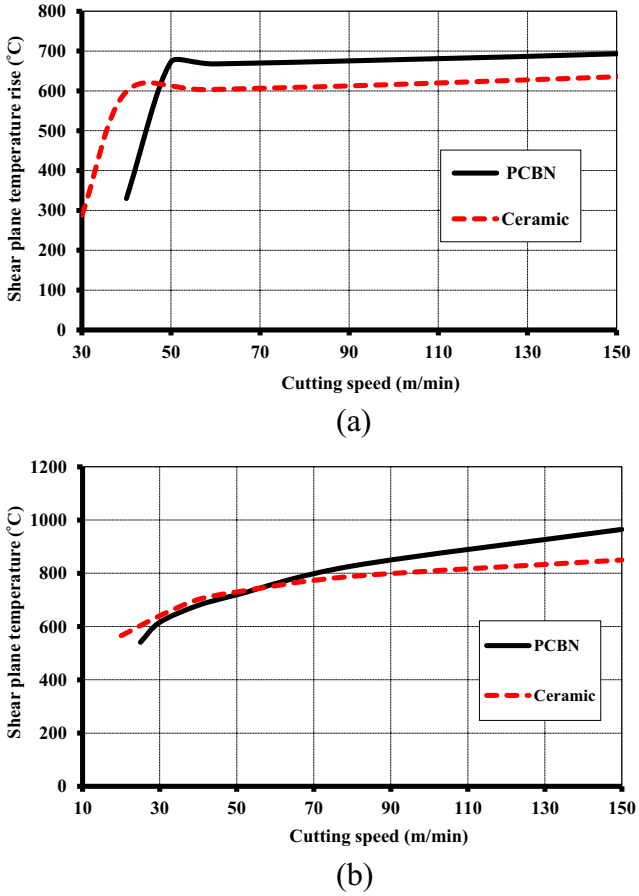

Fig. 10 Effect of the cutting speed (v) on the shear plane temperature rise (θ_s) in machining **a** HSS and **b** D2 tool steel, using ceramic and PCBN tools

showed higher shear plane temperatures during the higher speeds. These observations result from the variation of the proportion of the heat energy entering the chip through the shear plane (Γ_s) with the cutting speed. Γ_s is dependent on the shear strain (ε) that is a function of the chip compression ratio (λ_c). λ_c is affected by the tribological behavior at the tool-chip interface, which in turn depends on the cutting speed and the tool material [43].

Frictional temperature rise The effect of the cutting speed (v) on the frictional temperature (θ_f) when machining the HSS is illustrated in Fig. 11a. The ceramic tool produces a higher frictional temperature (θ_f) due to its low thermal conductivity (k_t). The same behavior is applied during machining of the D2 tool steel using the ceramic and PCBN tool materials (Fig. 13b). These observations can be confirmed by the results presented in Fig. 6.

In HSS, the frictional temperature rise values are greater than in the D2 tool steel, which can be attributed to the lower thermal conductivity of the HSS workpiece. This can be confirmed by Fig. 7.

3 Experimental work

Dry longitudinal turning tests were carried out on hardened (52 HRC) HSS and D2 workpiece materials. This hardness value is usually used for deep drawing, punching, and extrusion dies. A 3-kW digitally controlled general purpose lathe was used for the cutting tests.

PCBN and mixed alumina ceramic cutting tool inserts were mounted on a tool holder with − 6° rake angle, − 3° side rake angle, and − 9° back rake angle.

The tool-workpiece thermocouple was chosen for measuring the cutting temperature. Since only the potential difference was measured, it was enough to insulate a sole component of the circuit so that it did not affect the Machine-Fixture-Tool-Workpiece (MFTW) system rigidity to avoid chatter occurrence [20]. As insulating the workpiece would prove to be difficult, the tool holder was chosen instead. The preliminary tests showed that the MFTW system rigidity was not affected by the insulation on the tool holder. One of the lead wires was connected to the tool holder and the other directly to the tailstock. The direct machine connection (instead of slip rings or mercury path) would not affect the emf reading significantly [20]. Several tests were carried out to identify the effects of lead wire connected directly to the machine instead of the workpiece; no differences were observed, especially under limited length of cut. To overcome the parasitic emf problem, it was decided to avoid prolonged cutting. The response time of the tool-workpiece thermocouple was found to be approximately 0.25 s.

Both the tool post and the tool holder were completely insulated with silicone rubber. Al_2O_3 powder (2-μm particle size) was embedded into the rubber to increase its thermal stability against the hot chip. While measuring the cutting temperature under PCBN, the presence of another secondary junction between the CBN tip and the tungsten carbide substrate should be considered, which will decrease the measurement time to be within 5 s. The insert was completely insulated except for the CBN tip to prevent any contact between the chip and the tungsten carbide [44]. The presented cutting temperature is the mean values of three repetitive measurements with uncertainty of 5%.

A method was developed to calibrate the emf generated between the different types of tools and workpieces. A workpiece cylinder of 50 mm diameter and 50 mm length was prepared; a coned tip of 3 mm length was machined at the center of the cylinder. This cylinder was heated up to 1100 °C inside a heat treatment furnace. After heating up, the cylinder was connected to the center-drilled workpiece by inserting the cone inside the workpiece center-drilled hole. The other side of the workpiece was electrically connected to the voltmeter through the lead wire. The tool insert was mounted on the tool holder and connected to the other pole of the voltmeter. The lead wire connections at the workpiece and the tool holder were cooled to prevent any increase in their temperatures.

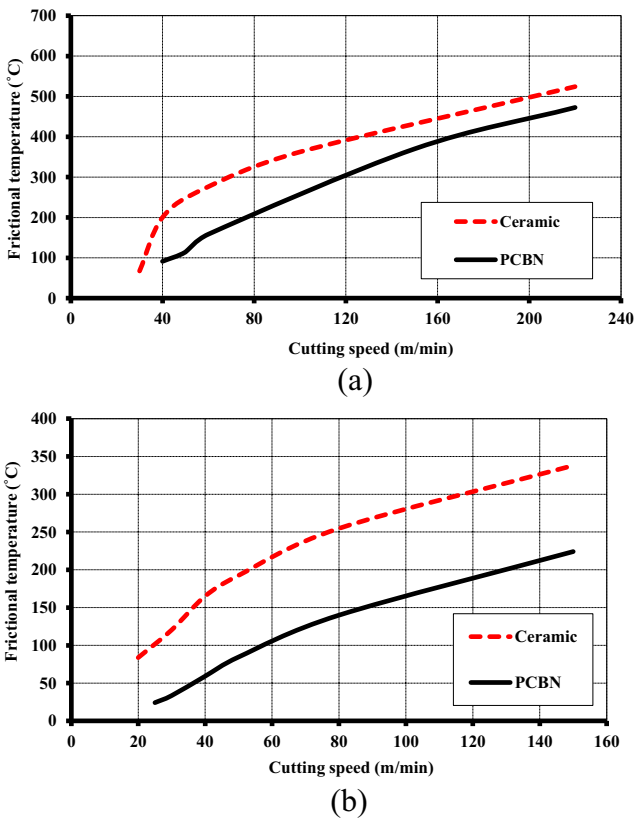

Fig. 11 Effect of the cutting speed (v) on the frictional temperature rise (θ_f) in machining **a** HSS and **b** D2 tool steel, using ceramic and PCBN tools

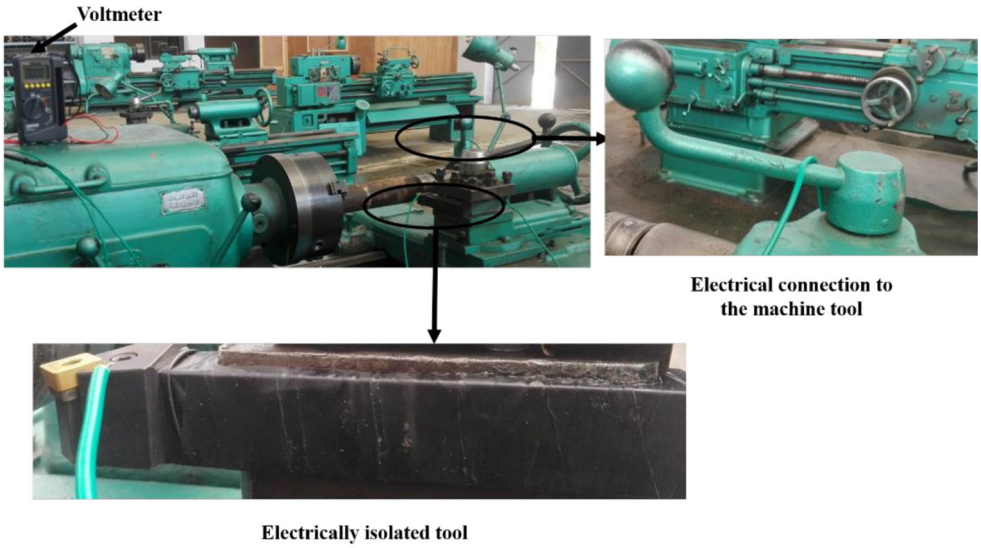

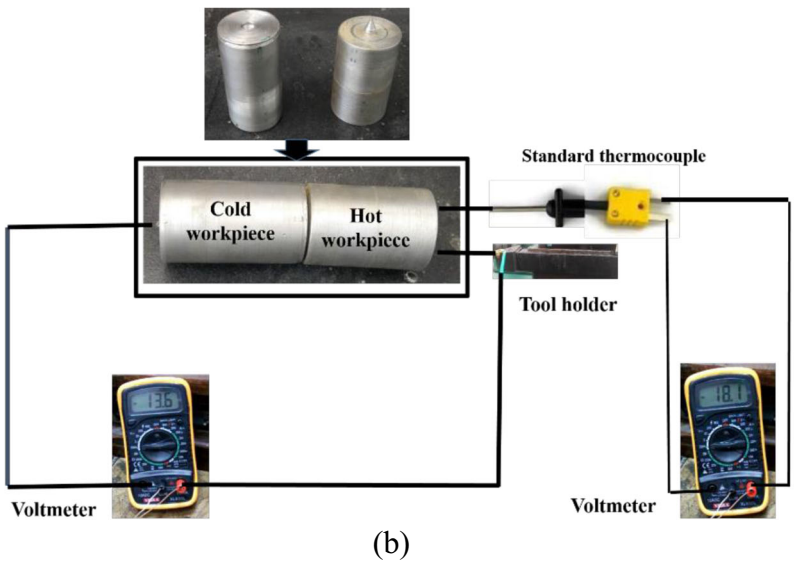

Fig. 12 Arrangement for **a** cutting temperature measurement and **b** the tool-workpiece thermocouple calibration

The emf generated between the tool and workpiece was compared to the emf signal of a precalibrated K-type thermocouple during the cooling down of the hot junction. The measurement and calibration arrangements are presented in Fig. 12. Cutting temperature measurements were carried out using fresh tools to avoid the effect of tool wear on the measured values. The used cutting conditions are summarized in Table 5.

Table 5 Used cutting conditions

Cutting conditions	Value
Cutting speed (v)	30–150 m/min for HSS and 10–150 m/min for D2 tool steel
Feed	0.1 mm/rev
Depth of cut range (a)	0.1 mm
Tool nose radius (r)	1.2 mm
Tool holder specifications	− 6° rake angle, − 3° side rake angle, and − 9° back rake angle, + 5° clearance angle
Time of cutting temperature measurement	3–10 s, depending on the cutting speed and tool material

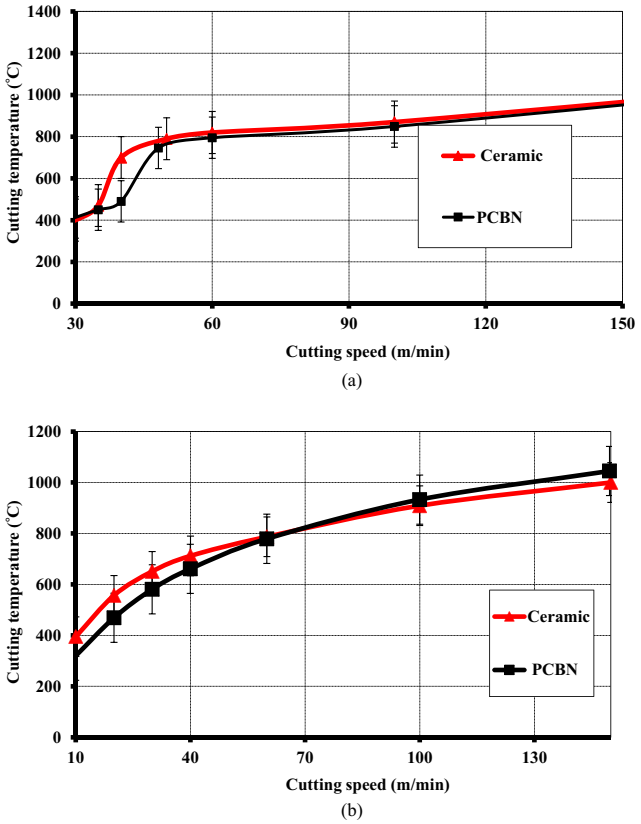

Fig. 13 Effect of the cutting speed (v) on the cutting temperature (θ_c) in machining **a** HSS and **b** D2 tool steel, using ceramic and PCBN tools

4 Results and discussion

Figure 13 shows the effect of the cutting speed (v) on the cutting temperature (θ_c) for the HSS and D2 tool steel.

For the HSS, the cutting temperature (θ_c) has increased from 400 to 750 °C within the cutting speed range of 30–50 m/min due to the effect of secondary hardening [40]. For the ceramic tools, this increase occurs in the range of 30–40 m/min, whereas for the PCBN cutting tool, in the range of 40–50 m/min. The delay at the start of secondary hardening of PCBN can be attributed to its higher thermal conductivity, leading to a relatively lower cutting temperature (θ_c) in the cutting speed range of 30–50 m/min. PCBN produces a lower cutting temperature than a ceramic tool at cutting speeds below 130 m/min. At greater cutting speeds ($v > 130$ m/min), the cutting temperature values of the ceramic tools are almost the same as for the PCBN tools.

D2 tool steel produces relatively higher cutting temperatures (θ_c) than the HSS due to its lower volumetric heat capacity ($\rho_w c_w$), resulting in higher shear plane temperatures (θ_s) as indicated in Figs. 3 and 4. PCBN exhibits lower cutting temperatures than the ceramic tool at cutting speeds of $v < 80$ m/min and almost the same temperatures at the higher cutting speeds.

However, the effect of the tool material thermal conductivity on the generated cutting temperatures becomes predominant at the lower cutting speed range. The identification of this range depends on the thermophysical properties of the workpiece material. If the cutting speed exceeds this range, the

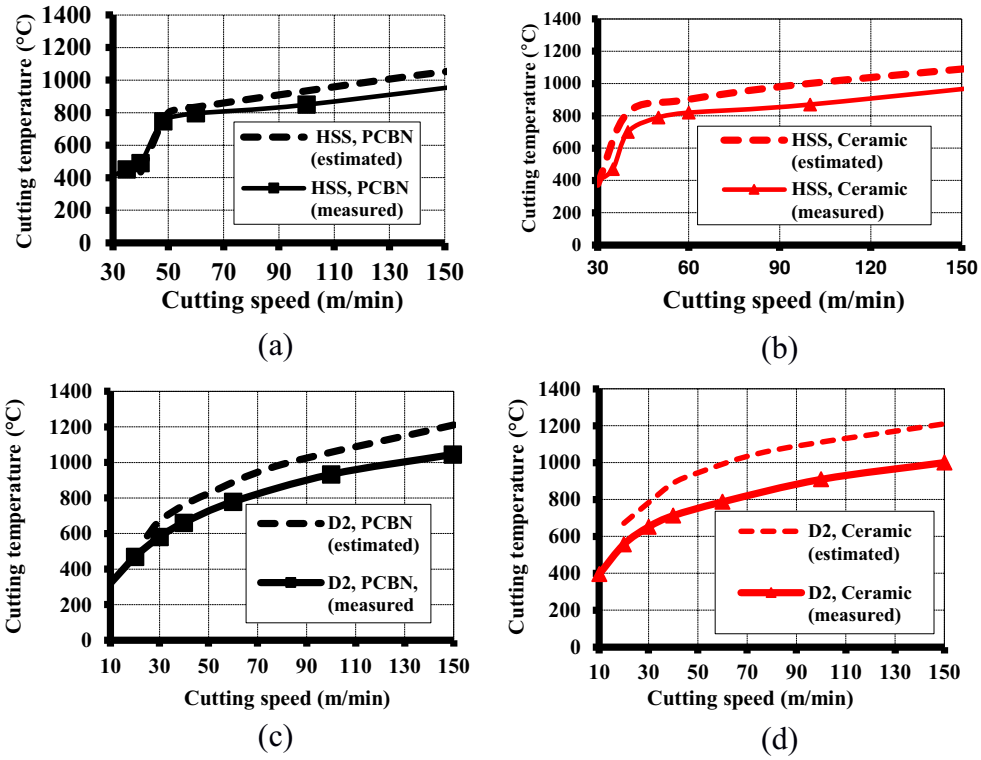

Fig. 14 Comparison between the measured and the estimated cutting temperatures when machining **a** HSS using PCBN tool, **b** HSS using ceramic tool, **c** D2 tool steel using PCBN tool, and **d** D2 tool steel using ceramic tool

effect of the tool material thermal conductivity on the cutting temperature becomes less remarkable.

Figure 14 presents the comparisons between the measured and estimated cutting temperatures of the HSS and D2 tool steel machined with the PCBN cutting tool. A maximum deviation of 20% can be observed between the estimated and measured values in all cases, which can be attributed to the uncertainties of the thermal properties of the used tool and workpiece materials, as well as the assumptions of the mathematical models.

5 Conclusions

A new thermal model for hard precision turning was established. The measured cutting force components, cutting variables (v, s, a), and the geometrical features of the cutting insert and tool holder were used to establish this model. Changes of thermophysical properties of the workpiece and tool materials with different temperatures were considered. The shear plane temperature and the chip frictional temperature rise (rake face temperature) can be deduced from the proposed model. It was observed that:

- A higher workpiece density decreases the shear plane temperature and does not remarkably affect the rake face temperature. Increasing the workpiece specific heat has the same effect as the workpiece density.
- Increasing the workpiece thermal conductivity decreases both the shear plane and the frictional temperature.
- Increasing the tool thermal conductivity decreases the frictional temperature and does not have a noticeable effect on the shear plane temperature.

Due to their relatively different thermophysical properties, hardened T15 HSS and D2 tool steels were used as workpiece materials in the present study. PCBN and mixed alumina ceramic tools were utilized to machine the selected workpiece material due to their different thermal conductivities. A tool-workpiece thermocouple system successfully measured the cutting temperature in hard precision turning.

For the HSS, the effect of secondary hardening can be observed through a sudden increase of the cutting temperature in the cutting speed range of 30–50 m/min. In ceramic tools, this jump occurs in the range of 30–40 m/min, whereas in the PCBN cutting tool, the jump takes place in the 40–50-m/min range, due to the latter's greater thermal conductivity leading to lower cutting temperatures.

D2 tool steel results in a relatively higher cutting temperature than the hardened HSS due to a lower volumetric heat capacity. Since density and specific heat are lower in the D2 steel, its shear plane temperatures are higher than those of the hardened HSS.

PCBN generates a lower frictional temperature than mixed alumina tools due to its greater thermal conductivity, which is in the range of 50–55 W/m °C (increasing with temperature), whereas the ceramic tool generates the highest frictional temperature due to a low thermal conductivity 23–13 W/m °C (decreasing upon a rise in temperature) in D2 and HSS machining.

The influence of the tool material thermal conductivity on the cutting temperatures becomes predominant at the lower cutting speed range. The increase of the cutting speed above this range reduces the magnitude of this effect.

A maximum deviation of 20% can be observed between the estimated and measured values of cutting temperatures in all cases, which may be attributed to the uncertainties of the thermal properties of the tool and workpiece materials as well as the assumptions of the mathematical model.

Funding This work was carried out at the Machining Research Laboratory, Faculty of Engineering, Ain Shams University, Cairo, Egypt. It was supported by Natural Sciences and Engineering Research Council of Canada (NSERC) under the Canadian Network for Research and Innovation in Machining Technology (CANRIMT) Strategic Research Network Grant NETGP 479639-15.

References

1. Komanduri R (1993) Machining and grinding—a historical review of classical papers. Appl Mech Rev 46:80–132. https://doi.org/10.1115/1.3121404
2. Abukhshim NA, Mativenga PT, Sheikh MA (2006) Heat generation and temperature prediction in metal cutting: a review and implications for high speed machining. Int J Mach Tools Manuf 46(7–8):782–800. https://doi.org/10.1016/j.ijmachtools.2005.07.024
3. Baohai W, Di C, Xiaodong H, Dinghua Z, Kai T (2016) Cutting tool temperature prediction method using analytical model for end milling. Chin J Aeronaut 29(6):1788–1794. https://doi.org/10.1016/j.cja.2016.03.011
4. Ng EG, Aspinwall DK (2002) The effect of workpiece hardness and cutting speed on the machinability of AISI H13 hot work die steel when using PCBN tooling. J Manuf Sci Eng 124(3):588–594. https://doi.org/10.1115/1.1452749
5. Kikuchi M (2009) The use of cutting temperature to evaluate the machinability of titanium alloys. Acta Biomater 5:770–775. https://doi.org/10.1016/j.actbio.2008.08.016
6. Díaz-Álvarez J, Cantero JL, Miguélez H, Soldani X (2014) Numerical analysis of thermomechanical phenomena influencing tool wear in finishing turning of Inconel 718. Int J Mech Sci 82:161–169. https://doi.org/10.1016/j.ijmecsci.2014.03.010
7. Devillez A, Le CG, Dominiak S, Dudzinski D (2011) Dry machining of Inconel 718, workpiece surface integrity. J Mater Process Technol 211:1590–1598. https://doi.org/10.1016/j.jmatprotec.2011.04.011
8. Díaz-Álvarez J, Tapetado A, Vázquez C, Miguélez H (2017) Temperature measurement and numerical prediction in machining Inconel 718. Sensors 17:1531. https://doi.org/10.3390/s17071531
9. Tönshoff HK, Arendt C, Ben Amor R (2000) Cutting of hardened steels. Ann CIRP 49(2):547–566. https://doi.org/10.1016/S0007-8506(07)63455-6

10. Shalaby MA, El Hakim MA, Abdelhameed MM, Krzanowski JE, Veldhuis SC, Dosbaeva GK (2014) Wear mechanisms of several cutting tool materials in hard turning of high carbon–chromium tool steel. Tribol Int 70:148–154. https://doi.org/10.1016/j.triboint.2013.10.011
11. Fox-Rabinovich G, Gershman I, Yamamoto K, Aguirre M, Covelli D, Arif T, Aramesh M, Shalaby M, Veldhuis S (2017) Surface/interface phenomena in nanomultilayer coating under severing tribological conditions. Surf Interface Anal 49(7):584–593. https://doi.org/10.1002/sia.6196
12. Ren XJ, Yang QX, James RD, Wang L (2004) Cutting temperatures in hard turning chromium hardfacings with PCBN tooling. J Mater Process Technol 147(1):38–44. https://doi.org/10.1016/j.jmatprotec.2003.10.013
13. Battaglia JL, Puigsegur L, Cahuc O (2005) Estimated temperature on a machined surface using an inverse approach. Exp Heat Transf 18(1):13–32. https://doi.org/10.1080/08916150590884826
14. Leshock CE, Shin YC (1997) Investigation on cutting temperature in turning by a tool work thermocouple technique. J Manuf Sci Eng 119(4A):502–508. https://doi.org/10.1115/1.2831180
15. Anagonye AU, Stephenson DA (2002) Modeling cutting temperatures for turning inserts with various tool geometries and materials. J Manuf Sci Eng 124(3):544–552. https://doi.org/10.1115/1.1461838
16. Bono M, Ni J (2002) A method for measuring the temperature distribution along the cutting edges of a drill. J Manuf Sci Eng 124(4):921–923. https://doi.org/10.1115/1.1511525
17. Ueda T, Al Huda M, Yamada K, Nakayama K, Kudo H (1999) Temperature measurement of CBN tool in turning of high hardness steel. CIRP Ann Manuf Technol 48(1):63–66. https://doi.org/10.1016/S0007-8506(07)63132-1
18. Al Huda M, Yamada K, Hosokawa A, Ueda T (2002) Investigation of temperature at tool-chip interface in turning using two-color pyrometer. J Manuf Sci Eng 124(2):200–207. https://doi.org/10.1115/1.1455641
19. Komanduri R, Hou ZB (2001) A review of the experimental techniques for measurements of heat and temperatures generated in some manufacturing processes and tribology. Tribol Int 34:653–682. https://doi.org/10.1016/S0301-679X(01)00068-8
20. Stephenson DA (1993) Tool-work thermocouple temperature measurements—theory and implementation issue. Transactions of the ASME, J Eng Ind-T Asme 115:432–437. https://doi.org/10.1115/1.2901786.20
21. Stephenson DA (1991) Assessment of steady-state metal cutting temperature models based on simultaneous infrared and thermocouple data. J Eng Ind 113(2):121–128. https://doi.org/10.1115/1.2899668
22. Stephenson DA, Agapiou JS (1997) Metal cutting theory and practice. Marcel Dekker, New York
23. Chen G, Ren C, Zhang P, Cui K, Li Y (2013) Measurement and finite element simulation of micro-cutting temperatures of tool tip and workpiece. Int J Mach Tool Manu 75:16–26. https://doi.org/10.1016/j.ijmachtools.2013.08.005
24. Maier T, Zaeh MF (2012) Modeling of the thermomechanical process effects on machine tool structures. Procedia CIRP 4:73–78. https://doi.org/10.1016/j.procir.2012.10.014
25. Nieslony P, Grzesik W, Laskowski P, Habrat W (2013) FEM-based modelling of the influence of thermophysical properties of work and cutting tool materials on the process performance. Procedia CIRP 8:3–8. https://doi.org/10.1016/j.procir.2013.06.056
26. Filice L, Umbrello D, Beccari S, Micari F (2006) On the FE codes capability for tool temperature calculation in machining processes. J Mater Process Technol 174:286–292. https://doi.org/10.1016/j.jmatprotec.2006.01.012
27. Umbrello D, Filice L, Rizzuti S, Micari F, Settineri L (2007) On the effectiveness of finite element simulation of orthogonal cutting with particular reference to temperature prediction. J Mater Process Technol 189(1–3):284–291. https://doi.org/10.1016/j.jmatprotec.2007.01.038
28. Komanduri R, Hou ZB (2000) Thermal modeling of the metal cutting process—part I: temperature rise distribution due to shear plane heat source. Int J Mech Sci 42(9):1715–1752. https://doi.org/10.1016/S0020-7403(99)00070-3
29. Komanduri R, Hou ZB (2001) Thermal modeling of the metal cutting process—part II: temperature rise distribution due to frictional heat source at the tool-chip interface. Int J Mech Sci 43(1):57–88. https://doi.org/10.1016/S0020-7403(99)00104-6
30. Moufki A, Molinari A, Dudzinski D (1998) Modeling of orthogonal cutting with a temperature dependent friction law. J Mech Phys Solids 46(10):2103–2138. https://doi.org/10.1016/S0022-5096(98)00032-5
31. Bahi S, Nouari M, Moufki A, El Mansori M, Molinari A (2011) A new friction law for sticking and sliding contacts in machining. Tribol Int 44(7–8):764–771. https://doi.org/10.1016/j.triboint.2011.01.007
32. Zhou F, Wang X, Hu Y, Ling L (2013) Modeling temperature of non-equidistant primary shear zone in metal cutting. Int J Therm Sci 73:38–45. https://doi.org/10.1016/j.ijthermalsci.2013.05.014
33. Li L, Li B, Ehmann KF, Li X (2013) A thermo-mechanical model of dry orthogonal cutting and its experimental validation through embedded micro-scale thin film thermocouple arrays in PCBN tooling. Int J Mach Tools Manuf 70:70–87. https://doi.org/10.1016/j.ijmachtools.2013.03.005
34. Shaw MC (2005) Metal cutting principles. Oxford University Press, New York
35. Polvorosa R, Suárez A, de Lacalle LNL, Cerrillo I, Wretland A, Veiga F (2017) Tool wear on nickel alloys with different coolant pressures: comparison of Alloy 718 and Waspalloy. J Manuf Process 26:44–56. https://doi.org/10.1016/j.jmapro.2017.01.012
36. Byrne G, Scholta E (1993) Environmentally clean machining processes—a strategic approach. CIRP Ann 42:471–474. https://doi.org/10.1016/S0007-8506(07)62488-3
37. Dudzinski D, Devillez A, Moufki A, Larrouquère D, Zerrouki V, Vigneau J (2004) A review of developments towards dry and high speed machining of Inconel 718 alloy. Int J Mach Tools Manuf 44:439–456. https://doi.org/10.1016/S0890-6955(03)00159-7
38. Canteli J, Cantero JL, Marín NC, Gómez B, Gordo E, Miguélez MH (2010) Cutting performance of TiCN-HSS cermet in dry machining. J Mater Process Technol 210:122–128. https://doi.org/10.1016/j.jmatprotec.2009.08.003
39. Shalaby MA, El Hakim MA, Veldhuis SC, Dosbaeva GK (2017) An investigation into the behavior of the cutting forces in precision turning. Int J Adv Manuf Technol 90(5–8):1605–1615. https://doi.org/10.1007/s00170-016-9465-8
40. El Hakim MA, Shalaby MA, Veldhuis SC, Dosbaev GK (2015) Effect of secondary hardening on cutting forces, cutting temperature, and tool wear in hard turning of high alloy tool steels. Measurement 65:233–238. https://doi.org/10.1016/j.2014.12.033
41. Abukhshim NA, Mativenga PT, Sheikh MA (2004) An investigation of the tool–chip contact length and wear in high-speed turning of EN19 steel. Proc Inst Mech Eng B J Eng Manuf 218:889–903. https://doi.org/10.1243/0954405041486064
42. Aleksandrovich AB, Danilenko BD, Loshchinin YV, Kolyadina TA, Khatsinskaya IM (1988) Thermophysical properties of low alloy high-speed steels. Metal Science and Heat Treatment 30(7):502–504. https://doi.org/10.1007/BF00777438
43. El Hakim M, Abad M, Abdelhameed M, Shalaby M, Veldhuis S (2011) Wear behavior of some cutting tool materials in hard turning of HSS. Tribol Int 44:1174–1181. https://doi.org/10.1016/j.triboint.2011.05.018
44. Dosbaeva GK, El Hakim MA, Shalaby MA, Krzanowski JE, Veldhuis SC (2015) Cutting temperature effect on PCBN and CVD coated carbide tools in hard turning of D2 tool steel. Int J Refract Metals Hard Mater 50:1–8. https://doi.org/10.1016/j.ijrmhm.2014.11.001